Polym. Bull. (2012) 69:375–388
DOI 10.1007/s00289-012-0759-1

ORIGINAL PAPER

Melt rheological properties of ETFE: an attempt to illuminate the fluorine-substitution effect

Xiao-Yong Chen · Wang Zhang Yuan · Fei Ai · Hong Li · Lei Li · Jing Wang · Yongming Zhang

Received: 14 October 2011 / Revised: 13 March 2012 / Accepted: 16 April 2012 /
Published online: 27 April 2012

Abstract Flow behaviors and rheological properties of ethylene tetrafluoroethylene alternating copolymer (ETFE) under high-shear conditions were first reported. Flow instabilities, shear and extensional viscosities, and die swell of ETFE were investigated. Rheological behaviors of perfluorinated ethylene propylene copolymers (FEP), partially fluorinated ETFE, and non-fluorinated polyethylenes (PE) were compared for understanding the role of fluorine incursion on materials properties. It is found that (1) ETFE does not have sharkskin region or second smooth region which frequently occurs in FEP and linear PE; (2) critical shear stresses at which surface melt fracture occurs for the three polymers follow the order: FEP < ETFE < PE; (3) stable flow region narrows, die swell weakens, and flow activation energy increases when fluorine content of polymer increases. After time–temperature superposition, shifted shear viscosity, extensional viscosity, and elastic data (die swell) present universal scaling characteristic and superpose well in term of the same shift factors.

Keywords ETFE · Shear viscosity · Extensional rheology · Die swell · Fluorine-substitution effect

X.-Y. Chen · W. Z. Yuan (✉) · F. Ai · H. Li · L. Li · Y. Zhang (✉)
School of Chemistry and Chemical Engineering, Shanghai Jiao Tong University, Shanghai 200240, People's Republic of China
e-mail: wzhyuan@sjtu.edu.cn

Y. Zhang
e-mail: ymzsjtu@yahoo.com.cn

X.-Y. Chen
School of Materials Science and Engineering, North University of China, Taiyuan 030051, People's Republic of China

J. Wang
Shangdong Dongyue Ltd, Zibo 256400, People's Republic of China

Abbreviations

D	Diameter of the die (mm)
L	Length of the die (mm)
Q	Volume throughout rate ($cm^3 \bullet s^{-1}$)
ΔP	Pressure drops (Pa)
ΔP_{ent}	Entrance pressure drops (Pa)
τ_a	Apparent shear stress (Pa)
τ_{tr}	True shear stress (Pa)
$\dot{\gamma}_a$	Apparent shear rate (s^{-1})
$\dot{\gamma}_{tr}$	True shear rate (s^{-1})
η	Shear viscosity (Pa s)
σ_e	Extensional stress (Pa)
$\dot{\varepsilon}$	Extensional deformation rate (s^{-1})
η_e	Extensional viscosity (Pa s)
η_0	Zero-shear viscosity (Pa s)
n	Non-Newtonian index
μ	Trouton ratio, $\mu = \frac{\eta_e}{\eta}$
α_T	Shift factor
B	Die swell ratio
ρ_s	Polymer density at ambient temperature, g cm^{-3}
ρ_m	Polymer density at test temperature, g cm^{-3}

Introduction

Alternating ethylene-tetrafluoroethylene copolymers (ETFEs) are widely used in aerospace, nuclear utilization, modern construction, and solar exploitation areas [1, 2] because of their high chemical and thermal resistance, flame retardancy, weathering, and electric insulation properties. Consequently, ETFEs are intensively explored on the molecular parameters and microstructures [3–9], thermal and crystallization behaviors [10–13], and steady-state viscous properties [14–16]. However, its capillary flow and high-shear rheological behaviors are scarcely reported, despite their fundamental and technical importance.

It is known that polymer rheological properties, particularly high-shear rheological characteristics, are closely related to their processing behaviors. Elucidating such features is thus essential for designing the forming processes and tailoring the product properties of the polymers. In addition, extensional viscosity plays an important role in fiber spinning, blow molding, and film blowing processes. Moreover, rheological information, particularly shear viscosity and modulus, can be constructed into master curves (scaling characteristic) via time–temperature superposition, giving rheological insights into the rheometry unreachable regions. Such scaling characteristic origins from the same relaxation mechanism in multiple hierarchy of polymer molecular motions. It is the inherent rheological nature of polymer fluids which is extensively reported [17, 18]. Actually, not only shear viscosity and modulus, but also elongational

viscosity and elastic properties for some polymers, such as polypropylene [19–21], can be superimposed into master curves, namely more extensive scaling characteristic in polymer flow behaviors.

Nowadays, advanced control is required in ETFE processing, making rheological properties inevitably needed for predicting the processing conditions and controlling its final product performances. In this paper, shear and extension rheological behaviors of ETFE were examined by capillary rheometer. The elastic feature was estimated using practical die swell and entrance pressure drop, and the critical melt fracture stresses of ETFE were determined based on the observation of extrudate appearance and cross-checked by the apparent flow curve technique etc. [22–24]. Meanwhile, universal scaling characteristics in ETFE melt flow are reported.

ETFE is made of alternated ethylene and tetrafluoroethylene segments. Comparison study on the rheological behaviors of perfluorinated ethylene–propylene copolymer (FEP), partially fluorinated ETFE, and nonfluorinated polyethylene will be helpful to understand the fluorine-substitution effect on polymer rheological and processing performances.

Experimental

ETFE resin granule (C88AX, Asahi Glass Company. LTD, Japan) was used. The melt flow rate of the resin is 9 g/10 min according to ASTM D 3159, and its molecular weight is 2.16 × 105 g/mol based on Tuminello et al.'s [9] rheological technique due to the insolubility of ETFE resin. The resin was dried at 80 °C for 2 h before high-shear extruding through a Rosand Rh10 capillary rheometer (Malvern Instruments, UK) equipped with a twin barrel which could obtain entrance effect directly. The measurements were carried out at 270, 280, 290, and 300 °C with the shear rates ranging from 47.8 to 6,500 s^{-1}. Diameter of long and orifice capillary dies are both 1 mm with a length to diameter ratio of 16 for the long die. Proper test temperature range was adopted to insure the polymers melted without degradation. A pre-heat for 12 min at 270 °C and 10 min at other temperatures was applied to release the pre-compression pressures caused by plunging piston. The melt fracture phenomena were observed by naked eyes and surface textures of the extrudates were pictured by camera. The die swell measurements were conducted by a vernier caliper (1-cm long extrudate, at least 5 extrudates) without considering the gravity effect.

The melt and crystallization behavior of C88AX was obtained through a DSC (Differential scanning calorimetry) thermal analyzer, Q100 (TA instruments, USA). The thermal scanning procedure, including melt and crystallization, follows below: (1) melt behavior, staying 5 min at −50 °C then heating (10 °C/min) to 350 °C; (2) crystallization behavior, ETFE was heated quickly (about 200 °C/min) to 350 °C and held 5 min at this temperature for removing thermal history, after that cooling with 10 °C/min to −50 °C.

Results and discussion

Melt and crystallization behavior of ETFE

For determining melt point and then selecting suitable extruding temperature, thermal analysis was performed (Fig. 1). The melt point of ETFE is about 242 °C, and crystallization point 259 °C. Figure 1 also shows that ETFE is a highly crystalline polymer, crystallinity level based on melt curve is 52.5 %, while on crystallization curve 49.2 %. In addition, we have confirmed that ETFE would degrade as temperature was above 300 °C [25]. Based on the above mentioned evidence, we select 270–300 °C as experimental temperature range.

Melt flow instabilities of ETFE

The melt flow instabilities (melt fractures or distortions) of ETFE are normally determined from extrudate appearance. When melt flow instabilities occurs, extrudates no longer maintain cylindrical shape or smooth surface [26, 27]. Figure 2 shows the extrudates images of C88AX collected at 280 °C from the 16 mm long die (photos at other temperatures are not presented here for concision) under different shear rates. Clearly, the melt flow instabilities became evident when the apparent shear rate is up to 365.4 s^{-1}. However, such steady flow region of ETFE is much broader than that of FEP which is below 70 s^{-1} under 350 °C [28], but narrower than that of linear polyethylene (about 500 s^{-1}) [29, 30]. It seems that stable flow region narrows with fluorine content.

Regular periodic drum patterns (not bamboo-like shape) were observed clearly on extrudates under the shear rates ranging from 489 to 876.8 s^{-1} (regular melt fracture). At higher shear rates, more complicated gross distortion textures (irregular melt fracture) appear. However, neither sharkskin region nor second smooth flow region emerged in our experiment. It is quite different from the linear polymer systems (*Note* for instance high density polyethylene, linear low density

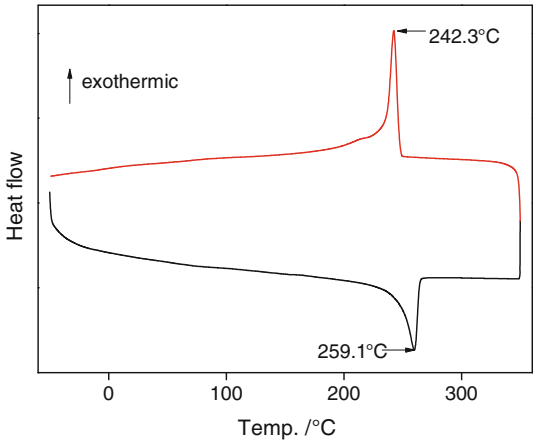

Fig. 1 Thermal behavior of C88AX

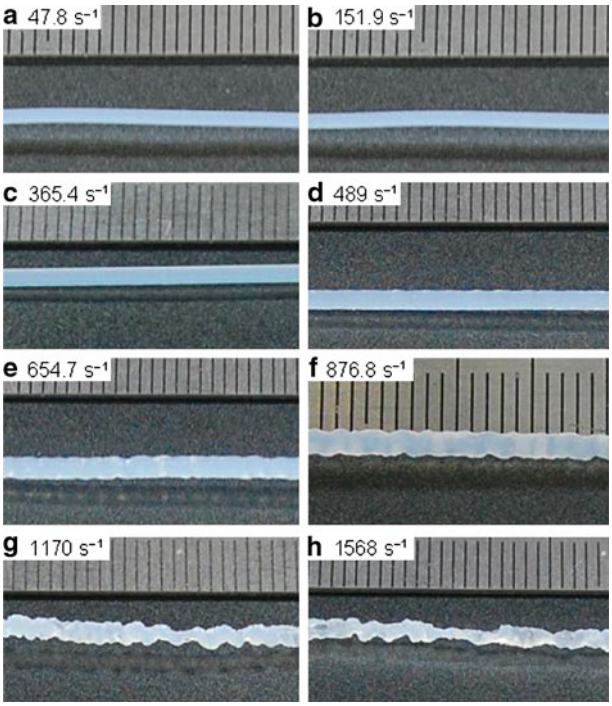

Fig. 2 Typical surface images of C88AX melts at 280 °C under different shear rates as indicated. The scale in the photos is a millimeter ruler

polyethylene, polybutadiene, polyisoprene, and linear polysiloxanes and fluorinated ethylene propylene copolymer, except polypropylene see Refs. [19, 26, 27]) where sharkskin region and second smooth flow region normally can be observed, but similar to the branched polymer systems [26], such as low density polyethylene (LDPE) [19, 22]. As temperature increased, the onset shear rates of melt fractures were promoted to much higher values (Table 1), implying wider processing window under elevated temperatures.

Table 1 The onset shear rates and shear stress of various flow regions for ETFE C88AX

Temp./°C	Regular pattern/s^{-1}		Irregular pattern/s^{-1}	
	$\dot{\gamma}_c$/s^{-1}	σ_c/MPa	$\dot{\gamma}_c$/s^{-1}	σ_c/MPa
270	365.4	0.28	654.7	0.33
280	489	0.23	1,170	0.32
290	876.8	0.27	2,803	0.35
300	1,170	0.30	3,749	0.41

$\dot{\gamma}_c$-critical shear rates where polymer extrusion mechanism changes take place

σ_c-critical shear stress where polymer extrusion mechanism changes take place

Apparent flow curve

The apparent flow curve, displaying the relationship between the apparent shear rate ($\dot{\gamma}_a = \frac{4Q}{\pi R^3}$) and apparent shear stress ($\tau_a = \frac{R\Delta p}{2L}$, where Q, R, and L are volume flow rate, radius, and length of the die, respectively), is frequently used to identify the initialization of flow instabilities and wall slips [17, 26] When flow instability arises, a slope discontinuity of the curve is frequently observed in FEP [28, 31], polyethylene [22, 23], polybutadiene [28], polyisoprene[19], and so on.

Figure 3 reports the apparent flow curves of C88AX at varying temperatures. Clearly, there are two slope breaks (marked by vertical dash lines) in the curves at relatively lower and higher shear rate regions, which are corresponded to the onset of the periodical and irregular melt fractures, respectively. It matches well with the surface textures observed by naked eyes. For example, the slopes of the curve for 280 °C are 0.52, 0.30, and 0.14 in the steady flow region, regular melt fracture region, and irregular melt fracture region (see solid lines in Fig. 3), respectively. Such slope variation amplitudes are similar to those of high-density polyethylene (HDPE) [23]. However, the steady flow slope of ETFE (0.52) is much closer to LDPE [23] (0.49) than to HDPE [23] (0.59), thus duly testifying ETFE is more similar to branched polymers. The apparent shear stress is monotonically increased with increasing apparent shear rate. Meanwhile, the slope at low shear rate region is higher than those at high-shear rate region, suggesting the increased non-Newton flow feature. This is a typical characteristic for polymers exhibiting shear thinning behaviors. In addition, the plot for 270 °C deviates remarkably from another three, which might be ascribed to the presence of unmelted crystal residues. Similar phenomena were also observed in FEP by Rosenbaoum and Koyama [28, 32].

It is also noticeable that in the higher shear rate end, viscosity reversion (high-temperature viscosity is larger than that at low temperature) occurs. Such reversion is mainly associated with melt fracture. When melt distortion happens, stress of

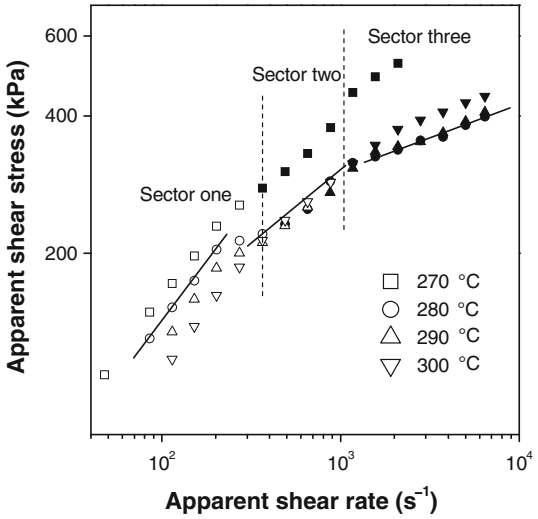

Fig. 3 The apparent flow curves of C88AX under different temperatures. The *filled symbols* represent melt flow instabilities

ETFE melts will instantly decrease, thus resulting in reduced apparent viscosity. Under lower experimental temperatures, melt fractures appear at lower shear rates where ETFE melts can flow stably under higher temperatures. As a result, under such rates, the shear viscosities under higher temperatures shift to higher values, giving viscosity reversions in the flow curves [28].

Entrance pressure loss versus true shear stress

Usually, the pressure drop in capillary extrusion involves entrance pressure loss (end effect) and pressure dissipation (true pressure drop in shear flow), which are caused by molecular chain extension and motion friction during flow through the die, respectively. The entrance pressure loss can be determined by Bagley correction [33]. Subsequently, the true pressure drop and true shear stress ($\tau_{tr} = \frac{(\Delta P - \Delta P_{ent}) \cdot R}{2L}$, where τ_{tr}, ΔP, and ΔP_{ent} are true shear stress, pressure drop, and entrance pressure loss, respectively) can be derived. However, nowadays, in practice, Bagley method is scarcely used and is substituted by zero-land die techniques [34].

The plot of entrance pressure loss at orifice die *vs* the true shear stress is usually used to characterize critical shear stress where flow instability starts. Such curves are more sensitive and accurate than apparent flow curves in identifying onset melt fracture [19, 21, 26]. As shown in Fig. 4, the entrance pressure loss showed two transitions, dividing the plots into three sectors. For example, two transitions at ~0.20 and 0.28 MPa were observed from the data at 280 °C, which are assignable to the regular melt fracture and irregular melt fracture beginning, respectively. However, the critical stress values mentioned above did not coincide with those obtained by observation of surface textures (see Table 1). The resolution and sensitiveness of naked eyes may not be high enough to distinguish finely flow mechanism changes like the mentioned technique.

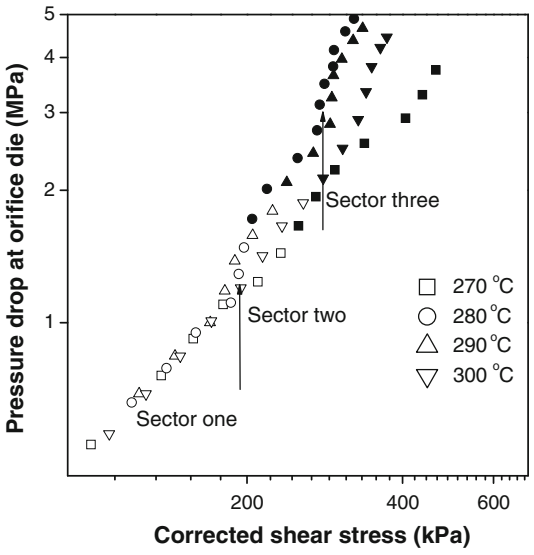

Fig. 4 Entrance pressure drop versus corrected shear stress of C88AX. The *filled symbols* represent melt fracture

The above first transition stress is higher than that of FEP(0.18 MPa) [28], but lower than that of linear low density polyethylene (LLDPE) (0.26 MPa) [22]. And the second transition stress is also far lower than that of LLDPE (0.43 MPa) [22, 23]. It can be concluded that the critical stress decreases with increasing fluorine content in polymers. The low adhesion and surface energy of fluorine-containing materials might be responsible to their lower critical stress [35]. The second critical transition of ETFE occurs approximately at the shear rate of 1,170 s^{-1}, which agrees with the visible irregular melt fracture beginning based on appearance observation (see Table 1). It is possible that naked eyes are more sensitive, and thus more accurate, to irregular melt distortion because the distortion beginning is much clearer than that of regular distortion.

The increasing rate of the entrance pressure loss in different sectors (Fig. 4) is according to the following order: sector one < sector two < sector three. It means that in the regular melt fracture region the energy loss is not so significant as that in the irregular fracture region, which is verified by the sharp increase of the entrance pressure loss and die swell (vide infra) in the latter case. The entrance pressure loss of C88AX melt decreases with the increasing temperature (from 280 to 300 °C). However, the plot for 270 °C does not follow this trend due to the earlier melt slip and fracture caused by the residual crystallites.

True shear viscosity

The determination of true shear viscosity begins from plotting the true shear stress (τ_{tr}) versus the apparent shear rate ($\dot{\gamma}_a$) on a double-logarithm scale. The plot slope (n) is adopted in the Rabinowitsch correction (non-Newtonian correction) [27]. Through the correction, the true shear rate ($\dot{\gamma}_{tr}$) on the capillary inner surface can be obtained according to Eq. 1:

$$\dot{\gamma}_{tr} = \frac{(3n+1)}{4n}\dot{\gamma}_a \tag{1}$$

Thereby, the true shear viscosity (η) can be determined as:

$$\eta = \frac{\tau_{tr}}{\dot{\gamma}_{tr}} \tag{2}$$

For most polymers, the shear viscosity at various temperatures can always be superposed into a master curve by use of the time–temperature superposition principle. Figure 5 shows the superposed true shear viscosity plot of ETFE shifted to 280 °C. The superposition was made based on Eq. 3 [18]:

$$\eta\left(\frac{\dot{\gamma}}{\alpha_T}\right)_{T_s} = \eta(\dot{\gamma})_T \tag{3}$$

where the left and right side represent shear viscosity at reference temperature T_s and temperature T, respectively. The shift factors were obtained based on its definition from linear viscoelasticity theory, namely $\alpha_T = \frac{\eta_{0T}}{\eta_{0T_s}}$ (the ratio of the zero-shear viscosity of T temperature vs. the zero-shear viscosity of T_s reference

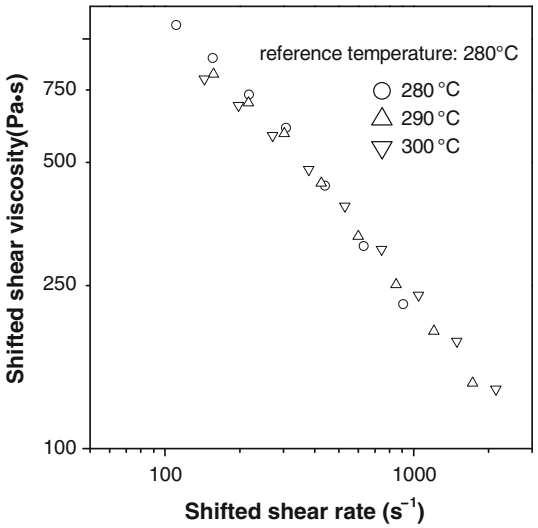

Fig. 5 Master curve of C88AX melts flowed through capillary die under 280 °C

temperature). Because capillary rheometry can not provide directly zero-shear viscosity, we employed the shear viscosity corresponding to the lowest shear rate investigated as alternative zero-shear viscosity and then corrected lightly through an adjustable coefficient for better superposition.

As shown in Fig. 4, the superposition is good (plot for 270 °C was not superposed due to the presence of residual crystallite). The shear viscosity demonstrates a strong shear-rate dependency, which supports the use of the Rabinowitsh correction. And the power law exponent of the shear viscosity for ETFE is 0.4 (derived from power law model). The shift factors are tabulated in Table 2. From which the activation energy of the shear flow was calculated to be 32.3 kJ/mol based on Arrhenius equation [27]. Such value is remarkably lower than those reported by Chu and co-worker [14] (64.26 kJ/mol) and Kostov and co-workers [15] (60 kJ/mol) under extremely low shear rate ($<1\ s^{-1}$). The difference may be derived partially from different ETFE resin compositions, and also partially from different flow mechanism under high and low shear rate [36]. According to the flow activation energy value, in an adiabatic flow, a temperature increase of 10 °C will result in a maximum decrease of shear viscosity by about 11 %. The energy of ETFE is lower than that of FEP (50 kJ/mol) [28], but slightly higher than that of HDPE (28 kJ/mol) [37], It suggests that polymer with higher fluorine fraction holds larger flow activation energy.

Extensional viscosity

By means of Binding and Cogswell's theory [38–41], extensional viscosity can be determined from entrance effect of the capillary rheometry. Several assumptions are made in their theory: first, the polymer melt adopts a coni-cylindrical flow pattern as it passes from the reservoir into the capillary to minimize the entrance pressure drop; second, the shear viscosity of the polymer melt can be described in terms of a

Table 2 Shift factors of ETFE melts under various temperatures

Temp./°C	280	290	300
α_T	1	0.96	0.94

power law model. Following the analysis, the extensional viscosity (η_e), extensional stress (σ_e), and extensional strain rate ($\dot{\varepsilon}$) were calculated as:

$$\eta_e = \left[\frac{3(n+1)\cdot\Delta P_{ent}}{4\sqrt{2}\cdot\dot{\gamma}_a}\right]^2 \cdot \frac{1}{\eta} \tag{4}$$

$$\sigma_e = \frac{3(n+1)\cdot\Delta P_{ent}}{8} \tag{5}$$

$$\dot{\varepsilon} = \frac{\dot{\gamma}_a}{2}\sqrt{\frac{2\eta}{\eta_e}} \tag{6}$$

The time–temperature superposed extensional viscosities of C88AX are shown in Fig. 6. The shift factors obtained from shear viscosity were also applied to extensional viscosities at varying test temperatures. Apparently, through superposition, the extensional viscosity plots overlapped well to form a master curve.

The calculated extensional viscosity range carries across one decade, with the magnitude varying between 3,000 and 17,800 Pa s (3–18 kPa s). In general, higher extensional viscosity brings higher melt strength, thereby better spinnability and drawability. The η_e of ETFE melt is remarkably higher than its corresponding shear viscosity, which is a common characteristic for polymer fluids [17, 36, 42], with the Trouton ratio ($\mu = \eta_e/\eta$, the ratio of extensional viscosity to shear viscosity [18]) ranging from 10 to 23. η_e of ETFE melt decreases with the increasing extensional

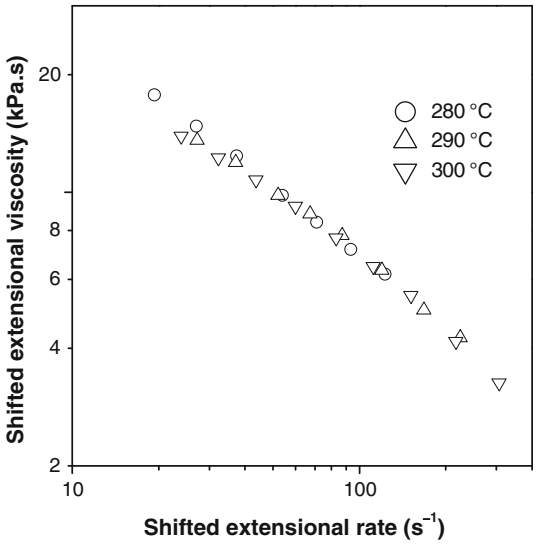

Fig. 6 Master curve of C88AX melts for the extensional viscosity data at varying extensional rates and temperatures

rate (tension thinning phenomenon), which can be ascribed to the disentanglement of macromolecular chains at high stretchings [18, 27, 43]. The η_e decrease can easily induce draw resonance during the melt-spinning processing process. Hence it is essential to control the processing conditions and/or resin parameters to prevent the η_e decrease and improve the spinnability of ETFE in fiber spinning or stretching-related process [44].

Die swell

Die swell data of C88AX at different temperatures are presented in Fig. 7**.** The die swell ratio (B) is normally determined as the ratio of the solid extrudate diameter (d) to the die the diameter (D). However, such method tends to underestimate the die swell of polymer fluids because of the shrinkage caused by cooling and/or crystallization. For more precise evaluation, a correction is conducted by multiplying the density ratio between test temperature and room temperature using Eq. 7 [21]:

$$B = \frac{d}{D} \times \frac{\rho_s}{\rho_m} \tag{7}$$

where ρ_s and ρ_m are polymer density at ambient temperature and test temperature, respectively. In addition, when melt fracture occurs, B increases and the extrudate diameters become heterogeneous. Therefore, the average diameter is determined from the measurements of mass of extrudates (at least 5 extrudates) with 1 cm length [19, 21, 45].

Die swell plots at different temperature are superposed into master curves by using the shift factors for shear viscosity with acceptable goodness. Similar die swell master curves are also seen in other polymer melts, such as polystyrene [46]

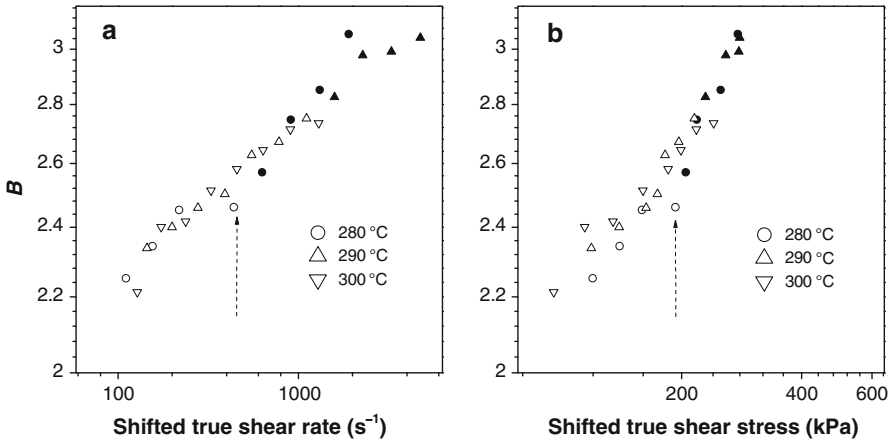

Fig. 7 Die swell master curves of ETFE melts for the data of **a** die swell ratio versus shear rate and **b** die swell ratio versus shear stress (using the shift factors of shear viscosity master curve, and the *filled symbols* represent melt fracture data)

and polypropylene[19]. It can also be observed that B increases continuously due to higher elastic energy in higher shear rate or shear stress. A slight slope change is observed at 0.19 MPa (Fig. 7b), which approaches to the critical shear stress of regular melt fracture obtained from the plot of entrance pressure drop versus corrected shear stress (0.20 MPa). The die swell ratios of ETFE melt increase with shifted shear rate because a higher shear rate provides larger elastic energy and shorter time for relaxation (Fig. 7a).

As Vlachopoulos [21] pointed out, die swell involves four components: Newtonian, elastic, inelastic, and relax. Theoretically, the contribution of the Newtonian is taken as a constant value of 0.12 [46]. The majority contribution of the die swell comes from the elastic component and at low shear region the contribution is 1.12. Herein, the die swell under the low shear end was close to 2.2 as seen in Fig. 7, which means large elasticity exists in ETFE melt even under low shear rates. When compared to FEP [47] and common polymers [19, 21, 45, 48, 49], the die swell ratio of ETFE is more closer to those of common polymers under same shear condition, implying different characteristics between partially fluorinated and perfluorinated polymers.

Conclusion

The flow behavior and rheological properties of ETFE confined in capillary die were first studied. With increased shear rate, the melt flow undergoes stable, regular fracture, and irregular fracture regions. Melt shear and extensional viscosities at varying temperatures are correlated well after time–temperature superposition and exhibit power law behaviors. Die swell ratios are increased with increasing true wall shear stress. The universal scaling characteristic in the high-shear flow behavior of ETFE is confirmed.

ETFE melt has no sharkskin region or second smooth flow region, which is more similar to branched polyethylene rather than linear polymers (such as high density and linear low density polyethylene). ETFE possesses wider stable flow region, lager die swell ratio, and higher critical melt fracture stress than perfluorinated FEP, but narrower stable flow region, slightly lower die swell, and lower critical stress than linear polyethylene. It may give us an implication that increased fluorine fraction in the polymer will result in narrower stable flow region, weakened die swell effect, higher flow activation energy, and lower critical melt fracture stress.

Acknowledgments We gratefully acknowledge financial supports from the "11th 5-year" National Key Technologies R&D Program of China (no. 2006BAE02A04) and the Shanghai Leading Academic Discipline Project (no. B202).

References

1. Zhang Y, Li H, Zhang H (2008) Fluorine-containing functional materials. Chemical Industry Press, Beijing
2. Drobny JG (2000) Technology of fluoropolymers. CRC Press, Boca Raton

3. Wu C, Buck W, Chu B (2002) Light scattering characterization of an alternating copolymer of ethylene and tetrafluoroethylene. 2. Molecular weight distributions. Macromolecules 20(1):98–103
4. Chu B, Wu C (2002) Light scattering characterization of an alternating copolymer of ethylene and tetrafluoroethylene. Macromolecules 19(4):1285–1286
5. Feng J, Chan C-M, Weng L-T (2000) Influence of chain sequence structure of polymers on ToF-SIMS spectra. Polymer 41(7):2695–2699
6. Phongtamrug S, Tashiro K, Funaki A, Arai K, Aida S (2008) Structural study of a series of ethylene-tetrafluoroethylene copolymers with various ethylene contents, Part 1: Structure at room temperature investigated for uniaxially-oriented samples by an organized combination of 2D-WAXD/SAXS and IR/Raman spectra. Polymer 49(2):561–569
7. Phongtamrug S, Tashiro K, Funaki A, Arai K (2008) Structural study of a series of ethylene-tetrafluoroethylene copolymers with various ethylene contents, Part 2: phase transition behavior investigated by temperature dependent measurements of X-ray fiber diagrams. Polymer 49(23): 5072–5083
8. Radice S, Del Fanti N, Zerbi G (1997) Phase transition in ethylene-tetrafluoroethylene(ETFE) alternating copolymer. A spectroscopic study. Polymer 38(11):2753–2758
9. Tuminello W, Buck W, Kerbow D (1993) Rheological molecular weight distribution determinations of ethylene/tetrafluoroethylene copolymers: implications for long-chain branching. Macromolecules 26(3):499–503
10. D'Aniello C, De Rosa C, Guerra G, Petraccone V, Corradini P, Ajroldi G (1995) Influence of constitutional defects on polymorphic behaviour and properties of alternating ethylene-tetrafluoroethylene copolymer. Polymer 36(5):967–973
11. Kostov G, Nikolov A, Atanassov A (2001) Study of the thermal properties and relaxation transitions in tetrafluoroethene-ethene copolymers. J Appl Polym Sci 81(11):2626–2632
12. Pucciariello R (1996) Melting behavior of ethylene-tetrafluoroethylene alternating copolymer. J Appl Polym Sci 59(8):1227–1235
13. Kostov G, Bogdanov B, Nikolov A (1994) Melting and crystallization of tetrafluoroethylene-ethylene copolymers. J Therm Anal Calorim 41(4):925–934
14. Kung L, Chu B (1995) Viscosity of ethylene tetrafluoroethylene alternating copolymers. Polymer 36(11):2265–2269
15. Nikolov AT, Dobreva AN, Georgiev DP, Kostov GK (1994) Rheological behaviour of the alternating tetrafluoroethylene-ethylene copolymer. Bulg Chem Commun 27(1):118–124
16. Wang Z, Tontisakis A, Tuminello W, Buck W, Chu B (1990) Viscosity characterization of an alternating copolymer of ethylene and tetrafluoroethylene. Macromolecules 23(5):1444–1446
17. Christopher WM (1994) Rheology: principles, measurements, and application. Wiley, New York
18. Ferry JD (1980) Viscoelastic properties of polymers, 3rd edn. Wiley, New York
19. Tao Z, Huang J (2003) Observation of melt fracture of polypropylene resins in capillary flow. Polymer 44(3):719–727
20. Huang Z, Zhang Y, Kotaki M, Ramakrishna S (2003) A review on polymer nanofibers by electrospinning and their applications in nanocomposites. Compos Sci Technol 63(15):2223–2253
21. Huang J, Tao Z (2003) Melt fracture, melt viscosities, and die swell of polypropylene resin in capillary flow. J Appl Polym Sci 87(10):1587–1594
22. Kalika DS, Denn MM (1987) Wall slip and extrudate distortion in linear low-density polyethylene. J Rheol 31(8):815–834
23. Ramamurthy AV (1986) Wall slip in viscous fluids and influence of materials of construction. J Rheol 30(2):337–357
24. Kurtz SJ (1984) Paper presented at the Advances in Rheology. In: Proceedings of the IX International Congress on Rheology, Universidad Nacional Autonoma de Mexico, Mexico
25. Chen XY, Yuan WZ, Zhao J, Yang L, Li H, Li L, Zhang Y (2012) Thermal-mechanical stability of ethylene tetrafluoroethylene alternating copolymer, and modification thereof. J Polym Res 19(2):1–6
26. Denn MM (2001) Extrusion instabilities and wall slip[J]. Annu Rev Fluid Mech 33(1):265–287
27. Han CD (1976) Rheology in polymer processing. Academic Press, New York
28. Rosenbaoum E (1998) Rheology and processability of teflon FEP resins for wire coating. The University of British Columbia, Vancouver
29. Kazatchkov IB, Yip F, Hatzikiriakos SG (2000) The effect of boron nitride on the rheology and processing of polyolefins. Rheol Acta 39(6):583–594
30. Sentmanat M, Hatzikiriakos SG (2004) Mechanism of gross melt fracture elimination in the extrusion of polyethylenes in the presence of boron nitride. Rheol Acta 43(6):624–633

31. Rosenbaoum EE, Hatzikiriakos S, Stewart C (1995) Flow implications in the processing of tetrafluoroethylene/hexafluoropropylene copolymers. Int Polym Proc 10(3):204–212
32. Kurose T, Takahashi T, Nishioka A, Masubuchi Y, Takimoto J-i, Koyama K (2003) The effect of pre-thermal history on shear and uniaxial elongational viscosity of a tetrafluoroethylene/hexafluoropropylene copolymer near the crystal melting transition. Rheol Acta 42(4):338–344
33. Bagley E (1957) End corrections in the capillary flow of polyethylene. J Appl Phys 28:624
34. Kim S, Dealy JM (2001) Design of an orifice die to measure entrance pressure drop. J Rheol 45:1413
35. Ebnesajjad S (2000) Fluoroplastics, vol 2—melt processible fluoropolymers. Plastics Design Library, New York
36. Haworth B, Gilbert M, Myers D (2005) Melt-state shear flow and elasticity of a thermoplastic fluorosulphonated—PTFE copolymer. J Mater Sci 40(4):955–964
37. Laun HM (1987) Orientation of macromolecules and elastic deformations in polymer melts. Influence of molecular structure on the reptation of molecules. Prog Colloid Polym Sci 75:111–139
38. Cogswell FN (1972) Measuring the extensional rheology of polymer melts. J Rheol 16(3):383–403
39. Cogswell FN (1969) Tensile deformations in molten polymers. Rheol Acta 8(2):187–194
40. Binding DM, Jones DM (1989) On the interpretation of data from converging flow rheometers. Rheol Acta 28(3):215–222
41. Binding DM (1988) An approximate analysis for contraction and converging flows. J Non-Newton Fluid 27(2):173–189
42. Martyn M, Nakason C, Coates P (2000) Measurement of apparent extensional viscosities of polyolefin melts from process contraction flows. J Non-Newton Fluid 92(2–3):203–226
43. Larson R (1995) The structure and rheology of complex fluids. Oxford University Press, Oxford
44. Chen K, Shen J, Tang X (2005) Rheological properties of poly (trimethylene terephthalate) in capillary flow. J Appl Polym Sci 97(2):705–709
45. Huang J, Leong K (2002) Shear viscosity, extensional viscosity, and die swell of polypropylene in capillary flow with pressure dependency. J Appl Polym Sci 84(6):1269–1276
46. Graessley WW, Glasscock SD, Crawley RL (1970) Die swell in molten polymers. J Rheol 14:519
47. Chen X-Y, Yuan W, Li H, et al. Rheological study on tetrafluoroethylene/hexafluoropropylene copolymer and its implication for processability[J]. J Appl Polym Sci. doi:10.1002/app.35665
48. Liang J (2009) Effects of extrusion conditions on melt viscoelasticity during capillary flow of low-density polyethylene. J Thermoplast Compos Mater 22(1):99–110
49. Thomas DP, Hagan RS (1969) The influence of molecular weight distribution on melt viscosity, melt elasticity, processing behavior and properties of polystyrene. Polym Eng Sci 9(3):164–171